Journal of Materials Chemistry A

Materials for energy and sustainability

rsc.li/materials-a

ROYAL SOCIETY
OF **CHEMISTRY**

PAPER
Hyunwoong Park *et al.*
Facilitating hole transfer on electrochemically synthesized p-type
CuAlO₂ films for efficient solar hydrogen production from water

PAPER

Check for updates

Facilitating hole transfer on electrochemically synthesized p-type CuAlO$_2$ films for efficient solar hydrogen production from water†

Seung Yo Choi,[ab] Chang-Duk Kim,[c] Dong Suk Han[d] and Hyunwoong Park [ID] *[abe]

Delafossite CuAlO$_2$ photoelectrodes are synthesized *via* the electrodeposition of Cu(II) and Al(III) onto fluorine-doped tin oxide (FTO) substrates in water and dimethylsulfoxide (DMSO) solvents, followed by annealing in air and Ar. The surface properties, crystalline structure, and photoelectrochemical (PEC) performance of the as-synthesized samples are significantly affected by the synthetic conditions. Optimized CuAlO$_2$ electrodes (synthesized in DMSO and annealed in air) possess suitable energetics for H$_2$ production under sunlight (an optical bandgap of ~1.4 eV and a conduction band level of −0.24 V$_{RHE}$). They exhibit a photocurrent onset potential of ~+0.9 V$_{RHE}$ along with a faradaic efficiency of ~70% at +0.3 V$_{RHE}$ in an alkaline solution (1 M KOH) under simulated sunlight (AM 1.5; 100 mW cm^{-2}). The addition of sacrificial hole scavengers (sulfide and sulfite) significantly improves the PEC performance of CuAlO$_2$ by a factor of eight, along with providing a faradaic efficiency of ~100%. This indicates that the hole transfer limits the overall PEC performance. This issue is addressed by employing a ~150 nm-thick Au film-coated FTO substrate for the CuAlO$_2$ deposition. In the absence of hole scavengers, the H$_2$ production with the Au-underlain CuAlO$_2$ photoelectrode (Au/CuAlO$_2$) is three-fold higher than that with bare CuAlO$_2$, while the faradaic efficiencies at +0.3 and +0.55 V$_{RHE}$ are ~100%. The time-resolved photoluminescence emission decay spectra of the CuAlO$_2$ and Au/CuAlO$_2$ confirm the facilitated charge transfer in the latter.

1. Introduction

The semiconductor-based solar production of carbon-neutral chemicals (*e.g.*, H$_2$ and formate from water and CO$_2$, respectively) has been studied over the past four decades,[1–4] but has recently received greater attention because of the increase in the concentration of atmospheric CO$_2$ beyond 400 ppm. There are numerous semiconductors available, including oxides,[5–9] chalcogenides,[10–13] silicon,[14–16] and III–V composites.[3,17] However, they often suffer from low efficiency, a complicated synthetic process, the use of expensive components, non-scalability, and low durability. Cu(I)-based delafossite materials are unique in terms of their structure (Cu^{I}M^{III}O$_2$ type, where M = Fe,[18–21] Rh,[22] Al,[23,24] Ga,[25] *etc.*); various bandgap (E_g) energies (1.2–3.0 eV);

high conduction band (E_{cb}) level, which is sufficient for H$_2$ production and CO$_2$ reduction; and relative stability in aqueous solutions compared to other p-type III–V and II–VI materials.[26,27] For example, electrodeposited *p*-CuFeO$_2$ (E_g ~ 1.36 eV) was shown to be capable of producing H$_2$ in an aqueous alkaline solution,[28] whereas intercalating Mg^{2+} or oxygen atoms into CuFeO$_2$ enhanced the photoelectrochemical (PEC) performance.[18] Furthermore, CuFeO$_2$ coupled with CuO (E_g ~ 1.4 eV) could produce formate from CO$_2$ and water at a circumneutral pH with a ~1% energy efficiency in the absence of any potential bias.[29–31]

In comparison to CuFeO$_2$, CuAlO$_2$ has been given less attention despite their similar physicochemical properties. The typical synthetic route of CuAlO$_2$ is annealing a Cu(I) and Al(III) salt mixture at high temperature (solid-solution process),[23,26] which results in irregular, coarse particles of several micrometers.[18,25] Although this method has some advantages (*e.g.*, high yield), the as-synthesized particles are difficult to fabricate into durable films on transparent conducting oxide (TCO) substrates because of the absence of particle-to-particle interaction. Even if they are formed, the films have less intimate and looser interparticle connections undergoing a significant charge recombination at the solid/solid interface.[18,23] This difficulty in synthesizing CuAlO$_2$ films has caused this material to be less studied despite its potential as a promising photocathode.

^{a}School of Energy Engineering, Kyungpook National University, Daegu 41566, Korea. E-mail: hwp@knu.ac.kr; Tel: +82-53-950-8973

^{b}School of Architectural, Civil, Environmental, and Energy Engineering, Kyungpook National University, Daegu 41566, Korea

^{c}Department of Physics, Kyungpook National University, Daegu 41566, Korea

^{d}Chemical Engineering Program, Texas A&M University at Qatar, Education City, P.O. Box 23874, Doha, Qatar

^{e}Advanced Institute of Water Industry, Kyungpook National University, Daegu 41566, Korea

† Electronic supplementary information (ESI) available: Fig. S1–S12. See DOI: 10.1039/c7ta01919j

This journal is © The Royal Society of Chemistry 2017

J. Mater. Chem. A, 2017, 5, 10165–10172 | **10165**

With this in mind, we have, for the first time, attempted to synthesize $CuAlO_2$ films on TCO substrates *via* electrochemical deposition (ED) under various experimental conditions (*e.g.*, ED potentials, times, solution media, and annealing atmospheres). The as-synthesized $CuAlO_2$ samples were characterized using various surface analysis tools (SEM, EDX, XRD, XPS, UV-vis, impedance, and time-resolved fluorescence spectrometry). They were then further evaluated in terms of their PEC hydrogen production in aqueous alkaline solutions under simulated sunlight (AM 1.5; 1 sun). The results of this evaluation showed that the hole transfer limited the overall PEC performance, and the use of sacrificial hole scavengers (electron donors) significantly improved the H_2 production. To address this issue, thin Au layers ($\sim$150 nm), as a hole conductor, were pre-deposited onto TCO substrates *via* an electron-beam evaporation system to facilitate the hole transfer of $CuAlO_2$. In the absence of the hole scavengers, the H_2 production with the Au-underlain $CuAlO_2$ photoelectrode ($Au/CuAlO_2$) was three-fold higher than that with bare $CuAlO_2$, while the faradaic efficiencies were $\sim$100%.

2. Experimental

2.1. Synthesis of samples

Pieces of fluorine-doped SnO_2 (F:SnO$_2$, FTO)-coated glass (Pilkington Co, 1 cm $\times$ 3 cm) were ultrasonically cleaned in ethanol for 10 min, rinsed with deionized water (>18 MΩ cm, Barnstead), and dried in an N_2 stream. For the electrochemical plating of Cu and Al, the as-prepared FTO (working electrode), saturated calomel electrode (SCE, reference electrode), and Pt wire (counter electrode) were immersed in a deionized water or dimethylsulfoxide (DMSO, >99%, Wako) solution containing $Cu(NO_3)_2 \cdot 3H_2O$ (4 mM, >99%, Sigma Aldrich), $Al(NO_3)_3 \cdot 9H_2O$ (20 mM, >98%, Sigma Aldrich), and $KClO_4$ (50 mM, >99%, Sigma Aldrich). Then, the FTO substrates were held at constant potentials (-0.31 V$_{SCE}$ in water and -1.91 V$_{SCE}$ in DMSO) for 2 h using a potentiostat/galvanostat (CompactStat, Ivium) (Fig. S1†). After the deposition, the samples were dried, washed with deionized water, and placed in a tube furnace (Ajeon Heating Industrial Co., LTD) at room temperature in the presence of atmospheric air or Ar. The furnace temperature was increased to 700 °C at a rate of 2 °C min^{-1} and held at 700 °C for 1 h. If necessary, Au-layered FTO (FTO/Au) was used for the deposition of $CuAlO_2$. For this, FTO substrates were coated with a 150 nm-thick Au layer using an electron-beam evaporation system (Dada Korea) with a metallic Au evaporation slug (99.999%) in a reactor chamber at a pressure of 2×10^{-5} Torr. The growth rate of the Au layer was estimated to be $\sim$0.05 nm s^{-1}.[32]

2.2. Photoelectrochemical measurements and product analysis

The as-synthesized samples (working electrodes) were immersed in aqueous potassium hydroxide (1 M KOH at pH $\sim$13.5, Sigma Aldrich) pre-purged with N_2 for over 1 h in an airtight single (undivided) glass cell with an SCE (reference electrode) and a platinum wire (counter electrode). Light-chopped linear sweep

voltammograms were obtained *via* a potential sweep from +0.3 to -0.9 V$_{SCE}$ at a scan rate of 5 mV s^{-1} under simulated solar light (100 mW cm^{-2}) from a 150 W xenon arc lamp (ABET Technology) equipped with an air mass (AM) 1.5G filter. The light intensity was weekly re-calibrated to be 1 sun (100 mW cm^{-2}) using a standard mono-Si solar cell (K801S-K009, McScience Inc.), as described elsewhere.[33] For the PEC H_2 production, constant potentials (-0.75 V$_{SCE}$ and -0.5 V$_{SCE}$) were applied to the samples under irradiation. The potentials of the reference electrode (SCE) were converted to those of a reversible hydrogen electrode (RHE) using the following relationship:

$$V_{RHE} = V_{SCE} + 0.241 + 0.059 \times pH$$

Unless otherwise specified, the RHE was omitted for simplicity. The incident photon-to-current efficiency (IPCE) was estimated using a CS130 monochromator (Mmac-200, Spectro) with a 300 W Xe arc lamp using the following equation:

$$IPCE\ (\%) = \frac{1240 \times I_{ph}\ (mA\ cm^{-2})}{P_{light}(mW\ cm^{-2}) \times \lambda(nm)} \times 100\%$$

where I_{ph}, P_{light}, and λ refer to the photocurrent densities at 0.3 and 0.55 V, photon flux, and wavelength, respectively.

For quantification of molecular hydrogen (H_2) evolved, varying volumes (10–250 μL) of a standard H_2 gas (99.999%) with Ar carrier gas were flowed through a 5 Å molecular sieve column equipped in a gas chromatograph (GC, YoungLin, ACME-6100) with a thermal conductivity detector (TCD) (detection limit of $H_2 \sim 0.01\%$), and a standard curve fit between the standard gas concentration and the corresponding spectral area was obtained. The faradaic efficiencies for H_2 under constant potentials were estimated using the following equation:

$$Faradaic\ efficiency\ (\%) =$$

$$\frac{H_2\ (mol) \times (6.02 \times 10^{23})}{\int_0^t I_{ph} dt \times A \times 1/96\,485\ \ C^{-1}\ mol \times t} \times 2 \times\ 100\%$$

where I_{ph}, A, and t are the photocurrent density (A cm^{-2}), area (0.25 cm^2), and time (s), respectively. All of the photoelectrochemical experiments were repeated at least twice to obtain reliable results.

2.3. Surface characterization

The surface morphologies and side views of the samples were analyzed using a field-emission SEM (FE-SEM, Hitachi S4800) equipped with an energy-dispersive X-ray (EDX) detector. The UV-vis diffuse reflectance absorption spectra of the powders collected from the sample films were obtained using a UV-vis spectrophotometer (UV-2450, Shimadzu), with $BaSO_4$ as a ref. 29. The obtained reflectance (R) was then converted into absorbance *via* the Kubelka–Munk function ($(1 - R)^2/2R$).[34] X-ray diffraction (XRD) measurements were performed to examine the crystalline structures of the samples with a Philips X-pert powder diffractometer (PW3040/00) in a Bragg–Brentano geometry under Cu Kα radiation. X-ray photoelectron

10166 | *J. Mater. Chem. A*, 2017, **5**, 10165–10172

This journal is © The Royal Society of Chemistry 2017

spectroscopy (XPS) and Auger spectroscopy (Cu LMM; XPS, ULVAC-PHI) analyses were performed on a PHI 5500 model spectrometer equipped with an Al Kα monochromator X-ray source at 20 kV, a hemispherical electron energy analyzer, and a multichannel detector. The time-resolved photoluminescence (TRPL) lifetimes were measured using a confocal microscope (MicroTime-200, Picoquant, Germany) with a 20× objective. The measurements were performed at the Korea Basic Science Institute (KBSI), Daegu Center, South Korea. A single-mode pulsed diode laser (379 nm with a pulse width of ∼30 ps and a laser power of ∼30 μW) was used as the excitation source. A dichroic mirror (Z375RDC, AHF), a long pass filter (HQ405lp, AHF), a 75 μm pinhole, a band-pass filter, and an avalanche photodiode detector (PDM series, MPD) were used to collect emissions from the samples. The details of the measurements and data analysis can be found elsewhere.[9,29,31,35]

3.   Results and discussion

3.1.   Electrochemical synthesis and characterization of CuAlO$_2$

Fig. 1 compares the light-chopped linear sweep voltammograms (LSVs) of samples that were electrochemically synthesized under diverse conditions. The sample deposited in the water solvent and annealed in an Ar atmosphere (water/Ar) showed a photocurrent onset potential (E_{on}) of ∼0.9 V and a significant dark current of E ∼0.45 V. In addition, there was a cathodic peak at ∼0.5 V, which was attributed to the reductions of Cu(I) and/or Cu(II) ($E°(Cu^{2+}/Cu^+) = +0.153$ V; $E°(Cu^+/Cu^0) = +0.521$ V). On the other hand, the sample deposited in water and annealed in an air atmosphere (water/air) exhibited a more anodic E_{on} (∼1.0 V) and yet large dark currents. The sample deposited in DMSO and annealed under Ar (DMSO/Ar) was poor at generating a photocurrent and suffered from a significant dark current. In contrast, the sample annealed in an air atmosphere (DMSO/air) displayed an E_{on} of ∼0.9 V and a high photocurrent. Furthermore, a dark current started from E ∼0.42 V, indicating that the sample is more durable than the other samples. The DMSO/Ar sample was yellowish, whereas the other samples were blackish. This suggests that the latter three samples possess similar compositions and/or crystalline structures.

The XRD patterns of the as-synthesized samples were further examined to gain knowledge about the crystalline structures (Fig. 2a). Most of the XRD peaks in the water/Ar sample were indexed to CuAlO$_2$ (e.g., 006, 101, 012, 009, 018, and 112 planes at $2\theta = 32.5°, 35.7°, 38.8°, 48.9°, 57.1°,$ and $68.1°$, respectively; JCPDS no. 73-9485), whereas there was a peak indexed to CuO (220) at $2\theta = 58.4°$. The water/air sample exhibited the same XRD pattern. In the DMSO/air sample, CuAlO$_2$ peaks were predominant, whereas the intensity of CuO (220) was significantly reduced. It should be noted that the Cu(I) in the Cu-based delafossites (Cu^{III}M^{III}O$_2$) is readily oxidized to Cu(II) in the synthesis process and/or a partial oxidation of CuAlO$_2$ in air, leading to oxygen-enriched oxides.[23,29,31] The presence of the mixed valence state of Cu(I) and Cu(II) usually increases the charge transfer.[19,31,36,37] In contrast to these samples, the DMSO/Ar sample did not exhibit CuAlO$_2$ peaks, whereas only Al$_2$O$_3$-associated peaks
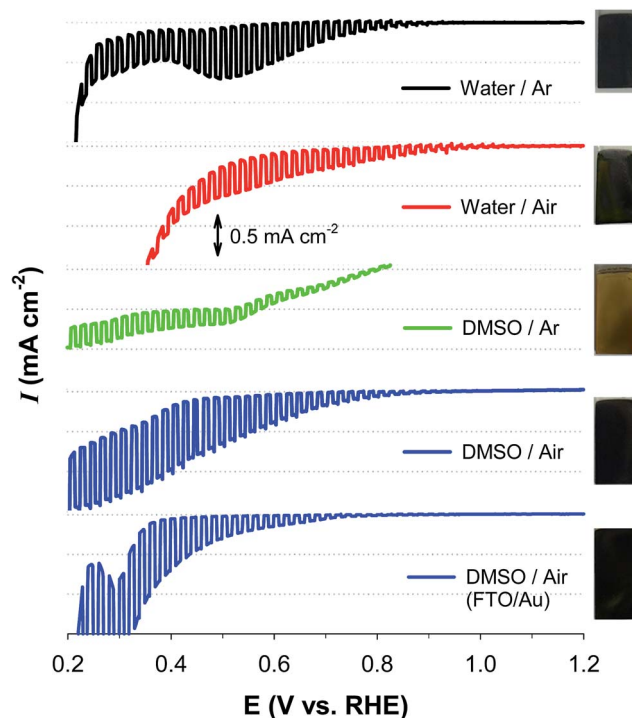

Fig. 1 Light-chopped linear sweep voltammograms (LSVs) of five sample electrodes synthesized via electrodeposition of Cu(II) and Al(III) onto FTO (omitted in legend) and FTO/Au in different solvents (water and DMSO) for 2 h followed by annealing in different atmospheres (air and Ar) at 700 °C. For example, DMSO/air refers to the sample deposited onto an FTO substrate in the DMSO solvent and annealed in an air atmosphere. Photos of the as-synthesized samples are shown on the right. FTO/Au refers to the FTO coated with a Au film (∼150 nm) via an electron-beam evaporation system. CuAlO$_2$ deposited onto the FTO/Au substrate is denoted as Au/CuAlO$_2$ in the text. To obtain the LSVs, the as-synthesized samples were immersed in an aqueous KOH solution purged with N$_2$ (1 M, pH ∼13.5) under irradiation of AM 1.5 (100 mW cm^{-2}).

(e.g., 111, 110, and 113 planes at $2\theta = 31.1°, 36.7°,$ and $43.6°$, respectively; JCPDS no. 75-0277) were found. This remarkable difference from the other samples was further confirmed by the yellowish color of the DMSO/Ar sample (Fig. 1).

Based on this knowledge, CuAlO$_2$ (i.e., the DMSO/air sample) was further analyzed using the XPS (Fig. 2b). The sample showed mixed bands at binding energies of 72 and 80 eV, the deconvolution of which indicated the co-presence of Al2p (73.6 eV) and Cu3p (74.9 and ∼76.8 eV) at an atomic ratio of 1 : 1. The EDX analysis of the sample confirmed the similar composition ratio (Fig. S2†). In addition, the XPS O1s band could be resolved into a single oxygen atom coordinated to Cu(I) at 529.6 eV and two oxygen atoms coordinated to Al(III) (one from the AlO$_6$ edge-sharing octahedral layer at 530.8 eV and the other from a surface hydroxide or hydrated species at 531.9 eV) (Fig. S3†). Two satellite peaks in the Cu2p spectrum further suggested the existence of Cu(II) (Fig. 2b),[33] which was consistent with the results of the XRD analysis. The presence of Cu(II) was further confirmed by the XPS spectra of the Cu LMM Auger transition (Fig. 2b inset). The as-synthesized CuAlO$_2$ sample exhibited
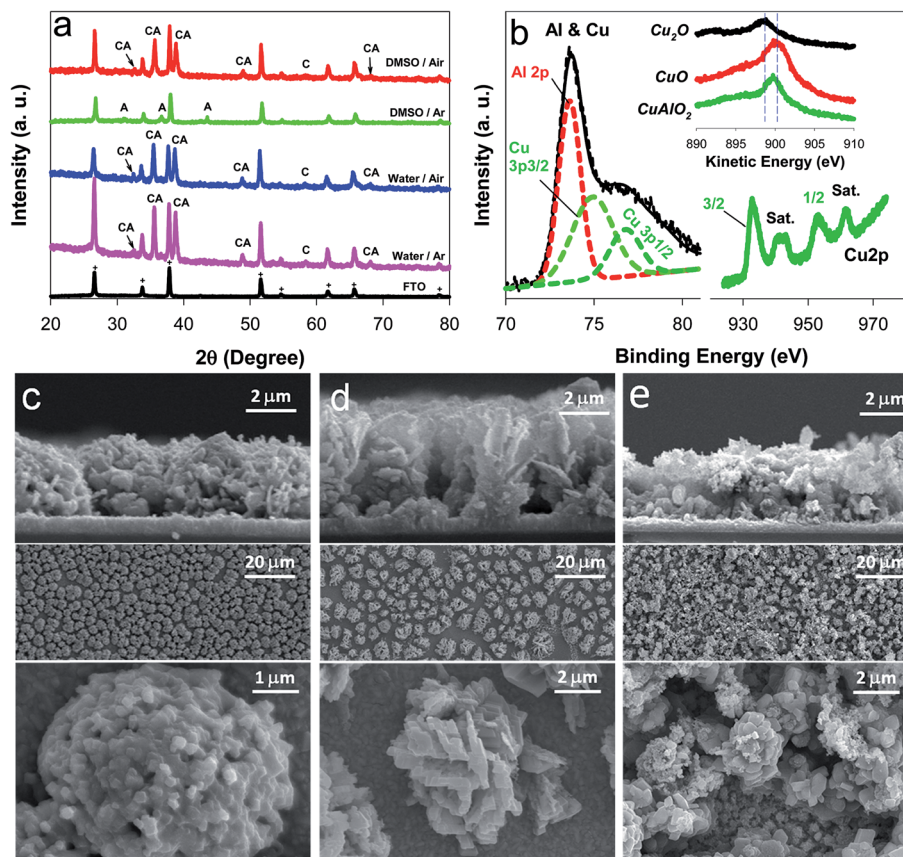
This journal is © The Royal Society of Chemistry 2017

J. Mater. Chem. A, 2017, 5, 10165–10172 | 10167

Fig. 2 Surface characterization of samples deposited onto FTO ((a) XRD, (b) XPS, and (c–e) SEM). In the XRD, CA, A, and C refer to $CuAlO_2$, Al_2O_3, and CuO, respectively (+originating from FTO). In the XPS of the DMSO/air samples, the left and right spectra show an Al2p and Cu3p mixed band (original and deconvoluted) and a Cu2p spectrum ($2p_{3/2}$, $2p_{1/2}$, and satellites), respectively, while the Cu LMM spectra of Cu_2O, CuO, and $CuAlO_2$ are compared in the inset. In the SEM, the cross-sectional and top views of (c) water/Ar, (d) water/air, and (e) DMSO/air are compared.

a kinetic energy peak at ~899.7 eV, which was located between those of Cu_2O (~898.8 eV) and CuO (~900.3 eV). The as-synthesized $CuAlO_2$ samples (*i.e.*, water/Ar, water/air, and DMSO/air) exhibited ~7 μm-thick porous particulate films composed of flower-like three-dimensional aggregates (Fig. 2c–e). This morphology is quite similar to those of electrochemically synthesized Cu-based oxide films ($CuFeO_2$, CuO, Cu_2O, *etc.*),[29–31] throughout which the component elements are uniformly distributed.[29,31] The elemental mapping of the $CuAlO_2$ confirmed the uniform distribution of Cu and Al horizontally and vertically in the sample (Fig. S4†).

3.2. Use of $CuAlO_2$ for photoelectrochemical H_2 production

The PEC hydrogen evolution with $CuAlO_2$ (*i.e.*, DMSO/air sample) was systematically examined in an alkaline electrolyte (1 M KOH) with sulfide and/or sulfite (0.1 M Na_2S, 0.1 M Na_2SO_3, and their mixed solution) as the sacrificial hole scavenger (Fig. 3a). It should be noted that sulfide and sulfite are typical products in the flue gas desulfurization processes of smelters and coal-fired power plants.[38] The overall shapes of the LSVs of the sulfide and sulfide/sulfite solutions were similar, with an E_{on} of ~0.85 V and a cathodic peak at ~0.45 V. When sulfite alone was present, a large dark current flowed at $E <$ ~0.7 V, whereas no cathodic peak was found. This suggests that the

cathodic peak of $CuAlO_2$ could be attributed to sulfide, which has a higher reducing power ($E°(S/S^{2-}) = -0.476$ V) than sulfite ($E°(S_2O_6^{2-}/H_2SO_3) = 0.564$ V). Despite the cathodic peak of the mixed solution, the dark current was inhibited down to an E value of ~0.37 V, which was 0.1 V more negative than that in water (Fig. 1d *vs.* Fig. 3a). In the absence of the hole scavengers, the application of a potential at +0.55 V did not produce H_2 for 3 h despite a photocurrent flow. We could observe measurable amounts of H_2 (~2.5 μmol for 3 h) only at $E \leq$ +0.3 V (Fig. 3b). A photocurrent of ~0.1 mA cm^{-2} was generated during the same period (Fig. S5†), leading to a Faraday efficiency of ~70% for H_2 production (Fig. 3c). In the presence of sulfite alone, the H_2 production and Faraday efficiency were enhanced yet insignificantly (~5 μmol for 3 h and ~80%, respectively). However, the addition of sulfide to the water and sulfite solutions markedly enhanced the H_2 production by ~7 and ~4 times, with Faraday efficiencies of ~90 and ~100%, respectively. Compared to sulfide alone, the higher efficiency of the sulfite/sulfide mixture was attributed to the regeneration of hole-oxidized sulfide (*e.g.*, S_2^{2-}) by sulfite.[10–12,39] The Faraday efficiency of ~100% with bare $CuAlO_2$ in the mixed solution reveals that electron injection at the p-type material/water interface was highly efficient, whereas the internal hole transfer limited the overall charge transfer (see below). For comparison, the PEC activities of the other samples
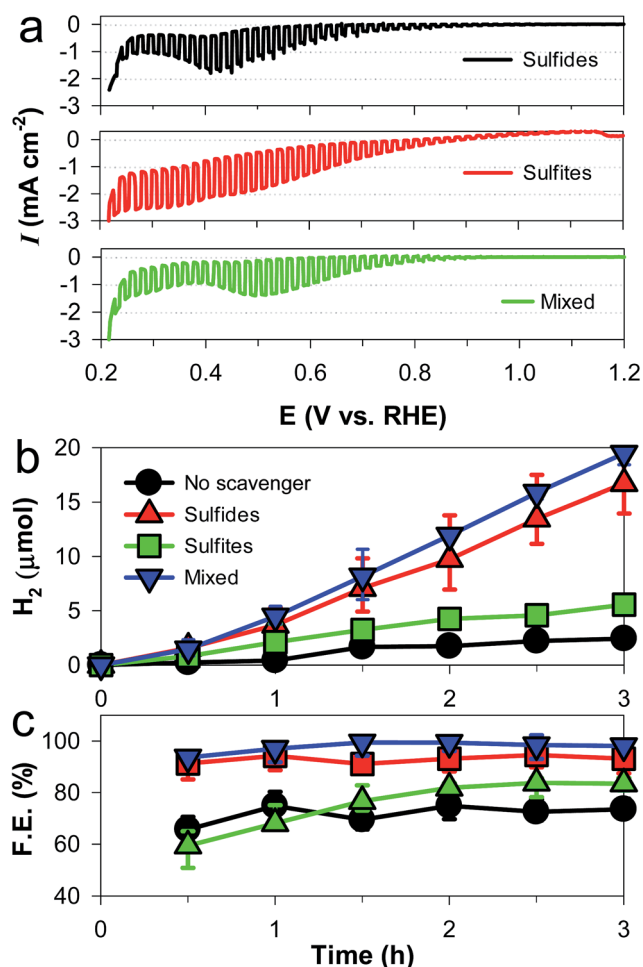
10168 | *J. Mater. Chem. A*, 2017, **5**, 10165–10172

This journal is © The Royal Society of Chemistry 2017

Fig. 3 Effects of hole scavengers (sulfide and/or sulfite, each 0.5 M) on the photoelectrochemical performance of $CuAlO_2$ electrodes in aqueous KOH solution (1 M) purged with N_2: (a) light-chopped LSVs, (b) H_2 production at +0.3 V_{RHE}, and (c) faradaic efficiencies (F. E.) for H_2 production at +0.3 V_{RHE}. "No scavenger" refers to 1 M KOH. See Fig. S5† for the photocurrent changes during the H_2 production tests.

(DMSO/Ar, water/Ar, and water/air) were examined in the mixed solution (Fig. S6†). The DMSO/Ar sample produced neither photocurrents nor H_2 at +0.3 V because of the predominant structure of Al_2O_3 (Fig. 2a). The other two samples with the

crystalline structure of $CuAlO_2$ exhibited the PEC activity; however, their H_2 production values were less than 5% of the production with the DMSO/air sample, and their faradaic efficiencies were less than 20%.

The energetics of the as-synthesized $CuAlO_2$ (i.e., DMSO/air samples) were examined in detail. The UV-vis diffuse reflectance absorption spectrum of the $CuAlO_2$ particles (collected from the films) showed a broadband light absorption in the wavelength range of 400–900 nm, and the bandgap (E_g) was estimated to be ~1.4 eV (corresponding to a λ value of ~885 nm; see Fig. 4a). This E_g value was attributed to the indirectly allowed transition of $CuAlO_2$ (1.2–1.7 eV),[23,40,41] whereas the directly allowed transition usually leads to large E_g values of 3–3.5 eV.[24,27] The indirect transition-induced photogeneration of charge carriers was confirmed by the IPCE profiles (Fig. 4a). The IPCE value at λ = 400 nm was estimated to be ~15% (E = +0.3 V; see Fig. 1 for the photocurrent profile), which was not only far greater than the value reported in the literature (~0% at λ > 400 nm) for $CuAlO_2$ synthesized via a sol–gel process[24] but also >2-fold greater than those of other copper-based delafossites (e.g., $CuFeO_2$ at E = +0.15 V) synthesized via the electrodeposition method.[29] In addition, the IPCE values decreased with increasing wavelength, with a wavelength onset of ~610 nm. A Mott–Schottky analysis of the as-synthesized $CuAlO_2$ film was performed at two frequencies (7 and 10 kHz) to estimate the flat band potential (E_{fb}) according to the following equation:[42]

$$\frac{1}{C^2} = \frac{2}{\varepsilon_0 \varepsilon_r e N_D}\left(E - E_{fb} - \frac{kT}{e}\right)$$

where C, ε_0, ε_r, N_D, E, k, and T refer to the space charge capacitance, permittivity of a vacuum, relative dielectric constant, donor density, applied potential, Boltzmann constant, and temperature, respectively. It should be noted that a decrease in $1/C^2$ with increasing potential bias is a characteristic of p-type semiconductors (Fig. 4b). The extrapolated x axis intercepts of the plots at the two frequencies coincided at E ~1.25 V, which corresponded to E_{fb}. Assuming that the valence band (VB) level was lower than E_{fb} by ~100 mV,[43] the conduction band (CB) of $CuAlO_2$ was determined to be −0.24 V, which is high enough to produce hydrogen from water ($E° = 0$ V) (Scheme 1a).

However, even though the energetics appeared to be suitable for PEC H_2 production, the as-synthesized $CuAlO_2$ generated
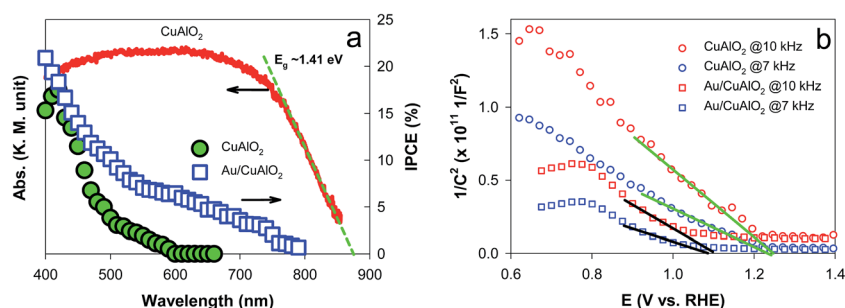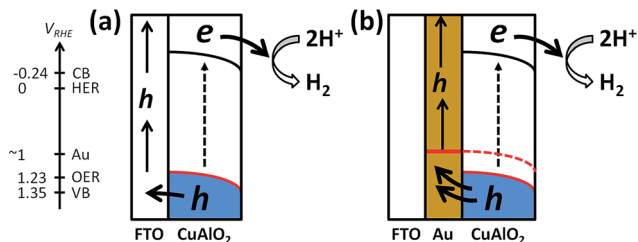

Fig. 4 (a) UV-vis diffuse reflectance absorption spectrum of $CuAlO_2$ particles (left) and incident photon-to-current efficiencies (IPCEs) of $CuAlO_2$ and Au/$CuAlO_2$ at +0.3 V_{RHE} in aqueous KOH solution (1 M) purged with N_2 (right). (b) Mott–Schottky plots of $CuAlO_2$ and Au/$CuAlO_2$ in aqueous KOH solution purged with N_2 (1 M).

This journal is © The Royal Society of Chemistry 2017

J. Mater. Chem. A, 2017, 5, 10165–10172 | **10169**

Scheme 1 Schematic band diagrams of CuAlO$_2$ deposited on (a) FTO and (b) FTO/Au substrates. An energy level arrow (left) shows the electrochemical potentials (*versus* the reversible hydrogen electrode, RHE) for the hydrogen evolution reaction (HER) and oxygen evolution reaction (OER), the conduction band and valence band (CB and VB, respectively) levels, and the work function (W_f) of Au. The W_f values (5.31–5.47 eV) were converted to the electrochemical potential.

a relatively small photocurrent density of ~0.1 mA cm^{-2} at 0.3 V in the absence of a hole scavenger (Fig. S5†). The addition of the hole scavenger enhanced the photocurrent density to ~0.6 mA cm^{-2} and the faradaic efficiency to ~100% (Fig. 3c), indicating that the hole transfer was limited. The hole transfer limit was straightforwardly examined by comparing the LSVs of the CuAlO$_2$ irradiated through the FTO substrate and electrolyte (Fig. S7†). Compared to the substrate-side irradiation, the electrolyte-side irradiation led to significantly reduced photocurrents, even though the light intensity arriving at CuAlO$_2$ in the substrate side-irradiation was ~80% of the reference light (AM 1.5G; 100 mW cm^{-2}) owing to the semi-transparent FTO (Fig. S8†).[33] Assuming the light penetration depth is the same between the two irradiation directions, the photogenerated holes and electrons under the electrolyte and substrate-side irradiations, respectively, must travel further than their counter charge carriers. Therefore, the reduced photocurrent in the electrolyte-side irradiation reveals that the hole transfer is limited compared to the electron transfer.

3.3. Facilitating hole transfer

To facilitate the hole transfer in water without hole scavengers, a 150 nm-thick Au film was overlaid onto FTO substrates *via* an electron-beam process, onto which CuAlO$_2$ was electrodeposited. The work function (W_f) of Au is 5.31–5.47 eV,[44] depending on the surface orientation, which can be estimated to be ~0.3 V more negative than the CuAlO$_2$ VB level (Scheme 1b). Accordingly, the Fermi level (E_F) equilibration between the W_f of Au and the E_F of CuAlO$_2$ causes an enhanced upward band-bending, leading to efficient hole transfer while inhibiting the electron–hole charge recombination. A comparison between the LSVs of the CuAlO$_2$ samples deposited on bare FTO and FTO/Au (denoted Au/CuAlO$_2$) showed that the E_{on} of the latter was ~0.1 V more negative than that of the former (Fig. 1) because of the upward shift in the E_F of the latter (Scheme 1b). In addition, the presence of the Au underlayer significantly inhibited the dark currents to E ~0.4 V (Fig. 1), while enhancing the photocurrents (Fig. S9†). The latter was further confirmed by the IPCE profile of Au/CuAlO$_2$, particularly in the range of $\lambda > $ ~450 nm (Fig. 4a). In contrast to the pristine sample, Au/CuAlO$_2$ exhibited an IPCE value of ~10%

at $\lambda = 500$ nm and IPCE onset at $\lambda = $ ~800 nm. These enhanced PEC properties could be attributed to the altered energetics produced by the Au underlayer. The Mott–Schottky plot of Au/CuAlO$_2$ showed an E_{fb} of ~1.1 V, which was approximately 0.15 V more negative than the E_{fb} of CuAlO$_2$ (Fig. 4b). Although slightly smaller than the estimated value of ~0.3 V, this shift qualitatively explains the enhanced upward band-bending.

Fig. 5a shows the PEC H$_2$ production values using Au/CuAlO$_2$ films at 0.3 and 0.55 V in an aqueous KOH solution (1 M) without the sulfide/sulfite hole scavengers. The H$_2$ production rate at 0.3 V was ~2.5 μmol h^{-1}, three-fold higher than the case of CuAlO$_2$ (Fig. 3b). The similar amounts of H$_2$ on the pristine CuAlO$_2$ at 0.3 V and Au/CuAlO$_2$ at 0.55 V (Fig. 3b *vs.* 5a) indicate that the deposition of the Au underlayer can save 0.25 V. Furthermore, the Au layer enhanced the photocurrent (Fig. S9†), while the faradaic efficiencies were similar (~100%) in these cases (CuAlO$_2$@0.3 V *vs.* Au/CuAlO$_2$@0.55 V) (Fig. 5b).
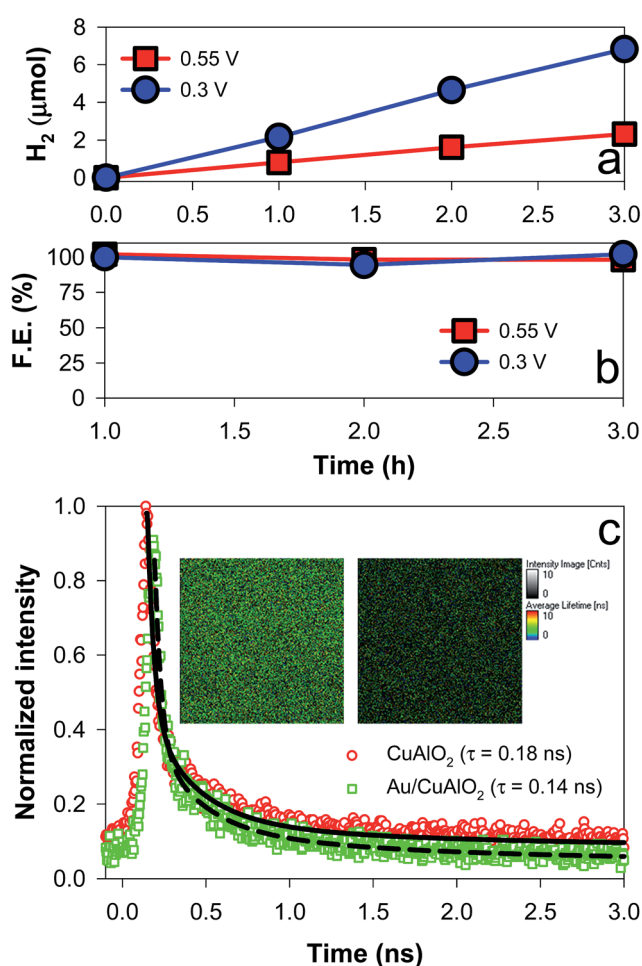

Fig. 5 (a) PEC H$_2$ production and (b) faradaic efficiencies using Au/CuAlO$_2$ electrodes at +0.3 V$_{RHE}$ and +0.55 V$_{RHE}$ in aqueous KOH solutions (1 M) purged with N$_2$. See Fig. S9† for the time-profiled changes in the photocurrents. (c) Time-resolved photoluminescence emission (500–700 nm) decay spectra of CuAlO$_2$ and Au/CuAlO$_2$. The average lifetime (τ) is also shown. The inset shows the 2D luminescence intensity and lifetime images of the samples. See Fig. S10–S12† for more information on the emission spectrum.

10170 | *J. Mater. Chem. A*, 2017, 5, 10165–10172

This journal is © The Royal Society of Chemistry 2017

Accordingly, it is obvious that the Au layer insignificantly influenced the electron injection at the $CuAlO_2$/water interface, while substantially enhancing the charge separation and transfer.

To examine the charge transfer kinetics and pathways, the time-resolved photoluminescence (TRPL) emission decay spectra of $CuAlO_2$ and $Au/CuAlO_2$ samples were compared (Fig. 5c). Prior to the TRPL analysis, the PL emissions of $CuAlO_2$ and $Au/CuAlO_2$ were examined in the range of $\lambda > \sim370$ nm (Fig. S10†). There were no specific emission bands, except for a band at ~470 nm. This band is usually found in other oxides and metals, and it could be attributed to the substrate and/or impurities. Accordingly, the samples were excited at $\lambda = 379$ nm, and the long wavelength emission (green emission of 500–700 nm) spectra were primarily compared (see Fig. S11† for the blue emission of 400–500 nm). Upon excitation, the emission intensities of both samples decayed exponentially on a nanosecond time scale, and the average decay time (τ) was estimated by fitting with exponential components (Fig. S11†). As a result, the τ of $CuAlO_2$ was found to be ~0.18 ns, which decreased to ~0.14 ns with the Au underlayer (Fig. 5c). When the instrument response was subtracted from the decay profiles, the τ values of $CuAlO_2$ and $Au/CuAlO_2$ were estimated to be 1.706 and 1.513 ns, respectively (Fig. S12†). This decrease in τ should have resulted from the charge transfer facilitated by the Au layer, leading to a reduction in the charge recombination. The emission intensity images in the inset of Fig. 5c further confirm the reduced charge recombination on the $Au/CuAlO_2$ film.

4. Conclusions

We demonstrated that a $CuAlO_2$ electrode could be readily synthesized *via* an electrodeposition process, and further attempted to enhance the PEC performance of the as-synthesized materials for H_2 production. Whereas $CuAlO_2$ displayed a similar morphology irrespective of the synthetic conditions (solvent and annealing atmosphere), the electroplating solvent significantly affected the surface properties, crystalline structure, and PEC performance of $CuAlO_2$. In an alkaline solution, the optimized $CuAlO_2$ samples showed an E_{on} value of ~0.9 V and H_2 production with a faradaic efficiency of $\sim70\%$ at 0.3 V. The addition of hole-scavengers (sulfide and sulfite) to the solution significantly improved the PEC H_2 production by a factor of 8, and led to a faradaic efficiency of $\sim100\%$. This strongly suggested that the hole transfer limits the overall PEC performance, which was confirmed by a comparison of the irradiation directions. To facilitate the hole transfer, $CuAlO_2$ was synthesized on an FTO substrate with a thin Au layer. In the absence of the hole scavengers, the H_2 production with $Au/CuAlO_2$ was three-fold that with $CuAlO_2$, while the faradaic efficiencies at 0.3 and 0.55 V were $\sim100\%$. The TRPL emission decay spectra of $CuAlO_2$ and $Au/CuAlO_2$ samples confirmed the facilitated charge transfer in the latter.

Acknowledgements

References

1 H.-J. Lewerenz and L. Peter, *Photoelectrochemical Water Splitting: Materials, Processes and Architectures*, The Royal Society of Chemistry, Cambridge, 2013.

2 K. Maeda and K. Domen, *J. Phys. Chem. Lett.*, 2010, **1**, 2655–2661.

3 F. E. Osterloh, *Chem. Soc. Rev.*, 2013, **42**, 2294–2320.

4 H. Park, H.-i. Kim, G.-h. Moon and W. Choi, *Energy Environ. Sci.*, 2016, **9**, 411–433.

5 J. K. Kim, G. Shin, S. M. Cho, T.-W. Lee and J. H. Park, *Energy Environ. Sci.*, 2011, **4**, 1465–1470.

6 S. K. Choi, S. Kim, S. K. Lim and H. Park, *J. Phys. Chem. A*, 2010, **114**, 16475–16480.

7 S. K. Choi, W. Choi and H. Park, *Phys. Chem. Chem. Phys.*, 2013, **15**, 6499–6507.

8 H. W. Jeong, S. Y. Choi, S. H. Hong, S. K. Lim, D. S. Han, A. Abdel-Wahab and H. Park, *J. Phys. Chem. C*, 2014, **118**, 21331–21338.

9 H. W. Jeong, W.-S. Chae, B. Song, C.-H. Cho, S.-H. Baek, Y. Park and H. Park, *Energy Environ. Sci.*, 2016, **9**, 3143–3150.

10 Y. K. Kim and H. Park, *Energy Environ. Sci.*, 2011, **4**, 685–694.

11 H. Park, Y. K. Kim and W. Choi, *J. Phys. Chem. C*, 2011, **115**, 6141–6148.

12 Y. K. Kim and H. Park, *Appl. Catal., B*, 2012, **125**, 530–537.

13 H. Park, H. H. Ou, A. J. Colussi and M. R. Hoffmann, *J. Phys. Chem. A*, 2015, **119**, 4658–4666.

14 S. K. Choi, U. Kang, S. Lee, D. J. Ham, S. M. Ji and H. Park, *Adv. Energy Mater.*, 2014, **4**, 1301614.

15 S. K. Choi, W.-S. Chae, B. Song, C.-H. Choi, J. Choi, D. S. Han, W. Choi and H. Park, *J. Mater. Chem. A*, 2016, **4**, 14008–14016.

16 K. Sun, X. Pang, S. Shen, X. Qian, J. S. Cheung and D. Wang, *Nano Lett.*, 2013, **13**, 2064–2072.

17 O. Khaselev and J. A. Turner, *Science*, 1999, **280**, 425–427.

18 J. Gu, A. Wutting, J. W. Krizan, Y. Hu, Z. M. Detweiler, R. J. Cava and A. B. Bocarsly, *J. Phys. Chem. C*, 2013, **117**, 12415–12422.

19 Y. J. Jang, Y. B. Park, H. E. Kim, Y. H. Choi, S. H. Choi and J. S. Lee, *Chem. Mater.*, 2016, **28**, 6054–6061.

20 M. S. Prévot, N. Guijarro and K. Sivula, *ChemSusChem*, 2015, **8**, 1359–1367.

21 O. Yehezkeli, N. M. Bedford, E. Park, K. Ma and J. N. Cha, *ChemSusChem*, 2016, **9**, 1–9.

22 J. Gu, Y. Yan, J. W. Krizan, Q. D. Gibson, Z. M. Detweiler, R. J. Cava and A. B. Bocarsly, *J. Am. Chem. Soc.*, 2014, **136**, 830–833.

23 N. Koriche, A. Bouguelia, A. Aider and M. Trari, *Int. J. Hydrogen Energy*, 2005, **30**, 693–699.

24 M. S. Prévot, Y. Li, N. Guijarro and K. Sivula, *J. Mater. Chem. A*, 2016, **4**, 3018–3026.

This journal is © The Royal Society of Chemistry 2017

J. Mater. Chem. A, 2017, **5**, 10165–10172 | **10171**

25 K. Gurunathan, J.-O. Baeg, S. M. Lee, E. Subramanian, S.-J. Moon and K.-J. Kong, *Catal. Commun.*, 2008, **9**, 395–402.

26 A. P. Amrute, Z. Lodziana, C. Mondelli, F. Krumeich and J. Perez-Ramirez, *Chem. Mater.*, 2013, **25**, 4423–4435.

27 I. Sullivan, B. Zoellner and P. A. Maggard, *Chem. Mater.*, 2016, **28**, 5999–6016.

28 C. G. Read, Y. Park and K.-S. Choi, *J. Phys. Chem. Lett.*, 2012, **3**, 1872–1876.

29 U. Kang, S. K. Choi, D. J. Ham, S. M. Ji, W. Choi, D. S. Han, A. Abdel-Wahabe and H. Park, *Energy Environ. Sci.*, 2015, **8**, 2638–2643.

30 S. Lee, U. Kang, G. Piao, S. Kim, D. S. Han and H. Park, *Appl. Catal., B*, 2017, **207**, 35–41.

31 U. Kang and H. Park, *J. Mater. Chem. A*, 2017, **5**, 2123–2131.

32 H. J. Kim, Y.-S. Sohn, C.-d. Kim and D.-h. Jang, *J. Korean Phys. Soc.*, 2016, **69**, 793–797.

33 N. C. Deb Nath, S. Y. Choi, H. W. Jeong, J.-J. Lee and H. Park, *Nano Energy*, 2016, **25**, 51–59.

34 H. Park, H.-H. Ou, U. Kang, J. Choi and M. R. Hoffmann, *Catal. Today*, 2016, **266**, 153–159.

35 S.-H. Hwang, Y. K. Kim, S. H. Yoon, S. K. Lim and H. Park, *RSC Adv.*, 2016, **8**, 85521–85528.

36 P. Wang, Y. H. Ng and R. Amal, *Nanoscale*, 2013, **5**, 2952–2958.

37 Y. Yang, D. Xu, Q. Wu and P. Diao, *Sci. Rep.*, 2016, **6**, 35158.

38 N. de Nevers, *Air Pollution Control Engineering*, McGraw-Hill, New York, 1995.

39 H. Park, W. Choi and M. R. Hoffmann, *J. Mater. Chem.*, 2008, **18**, 2379–2385.

40 R. Brahimi, M. Trari, A. Bouguelia and Y. Bessekhouad, *J. Solid State Electrochem.*, 2010, **14**, 1333–1338.

41 N. Benreguia, S. Omeiri, B. Bellal and M. Trari, *J. Hazard. Mater.*, 2011, **192**, 1395–1400.

42 T. H. Jeon, A. D. Bokare, D. S. Han, A. Abdel-Wahab, H. Park and W. Choi, *Appl. Catal., B*, 2017, **201**, 591–599.

43 S. R. Morrison, *Electrochemistry at Semiconductor and Oxidized Metal Electrodes*, Springer, New York, 1980.

44 D. R. Lide, *CRC Handbook of Chemistry and Physics*, CRC Press, New York, 90 edn, 2009.